Fluorescence nanotomography–a structural tool in biomedical sensing

Olaf J Rolinski[#] and David J S Birch
Photophysics Research, Deptartment of Physics, University of Strathclyde

ABSTRACT

Fluorescence nanotomography (FN) is a newly developed method for determining molecular distributions on a nanometre scale in soft solids, biological macromolecules and medically important systems. FN uses fluorescence resonance energy transfer (FRET) for the recognition of the separations between molecules. By using a fluorescence lifetime measurement of sub-nanosecond time resolution, the spatial resolution of the resulting distribution function can be better than 1 Å. In this paper the theoretical background of the method is outlined and the results of simulations on model molecular distributions presented. This is followed by demonstration of several applications of FN to real molecular systems, including bulk solutions of molecules of different sizes, complexes, porous polymers, phospholipids and sugar-protein competitive binding sensors glucose. The experimental requirements of FN as a structural tool for wide class of biomedical systems are discussed.

Keywords: fluorescence sensors, FRET, fluorescence lifetime measurement.

1. INTRODUCTION

Determining the nano-morphology of colloidal and macromolecular structures and molecular sensors plays an increasingly important role in environmental sciences and industry as well as in biomedical applications. Among several methods adopted for gaining structural information when radiation interacts with nanoscale units, (e.g. x-ray crystallography, NMR spectroscopy, light microscopy, to name just a few), fluorescence spectroscopy is especially useful in structural sensing. This is because of its numerous advantages, including in-situ nature, high spatial resolution, non-invasiveness, high sensitivity and specificity and opportunity for remote sensing. The dye-environment interactions, well researched in the past in numerous solution-based experiments, are now used to gain molecular information in more complex systems, such as membranes, polymers, proteins and gels.

Each structural fluorescence sensor is based on a specific structure-sensitive and fluorescence-related mechanism. Fluorescence resonance energy transfer (FRET) is extremely useful here, as the rate of FRET is strongly distance dependent ($k(r) \sim r^{-6}$). Consequently, the fluorescence decay of the initially excited molecule (donor) affected by FRET to another molecule (acceptor) will depend on the donor-acceptor separation. This is a background for sensing applications of FRET, including the fluorescence nanotomography (FN) approach, described in this paper.

According to Förster theory [1], FRET is a non-radiative path of depopulation of the donor excited state (Fig.1a) and its rate $k(r)$ is given by

$$k(r) = \frac{1}{\tau_0}\left(\frac{R_0}{r}\right)^6 \qquad (1)$$

where r is a donor-acceptor separation, τ_0 is a donor fluorescence lifetime in the absence of the acceptor and R_0 is a critical Förster distance, given by the overlap integral

[#] o.j.rolinski@strath.ac.uk; phone 44 141 548 4230; fax 44 141 552 2891; http://www.phys.strath.ac.uk/Groups/groups.html, Photophysics Group, Department of Physics, University of Strathclyde, John Anderson Building, 107 Rottenrow, Glasgow G4 0NG, Scotland, UK;

Opto-Ireland 2002: Optics and Photonics Technologies and Applications, Thomas J. Glynn, Editor, Proceedings of SPIE Vol. 4876 (2003) © 2003 SPIE · 0277-786X/03/$15.00

$$R_0^6 = \frac{9000 \ln(10) \mathrm{K}^2 \Phi_0}{128 \pi^5 N_A n^4} \int_0^\infty \frac{F_d(\tilde{\nu}) \varepsilon(\tilde{\nu})}{\tilde{\nu}^4} d\tilde{\nu} \qquad (2)$$

Here Φ is the donor fluorescence quantum yield in the absence of acceptor and n is the refractive index of the solvent. $F_D(\tilde{\nu})$ represents the normalised fluorescence spectra of the donor and $\varepsilon_A(\tilde{\nu})$ is the molar absorption coefficient of the acceptor. κ^2 is the orientational factor equal to 2/3 for fast and freely rotating donor and acceptor molecules.
It follows from Eqtn (2), an overlap between the donor fluorescence and acceptor absorption spectra (Fig.1b) is necessary for FRET to occur. This condition provides an opportunity for reaching high sensitivity of the donor for the specific acceptor (good spectral overlap) and selectivity (poor overlap with other fluorophores).

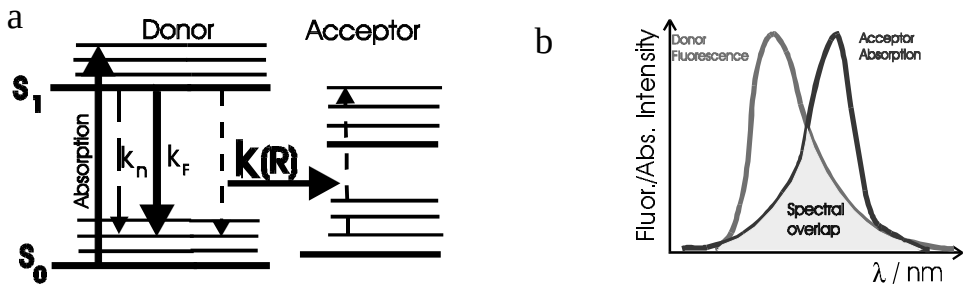

Fig. 1. The principle of FRET between donor and acceptor molecule. The resonance condition is expressed by a non-zero overlap between donor fluorescence and acceptor absorption spectra.

The simplest sensing application of FRET consists of detecting the presence of the acceptor by monitoring changes in donor lifetime and/or quantum yield [2]. In this case a relevant calibration curve can be found and used to estimate the concentration of acceptor, but no structural information can be recovered.

Our task is to determine the structure of a system from its fluorescence. This constitutes an inverse problem where the object (molecular structure) has to be determined from its image (fluorescence characteristics). In this type of problem [3], the image does not contain enough information for full reconstruction of the object, thus some additional information is required prior to experiment. This prior information can be the result of another experiment, parameters of the experimental set-up, or/and assumptions regarding expected form of the object. An adequate choice of this information and their appropriate use in data analysis are crucial when we try to extract full structural information from the lifetime data.

The most commonly used prior information in the lifetime FRET based sensing is an assumption for the donor-acceptor distribution function $\rho_{DA}(r)$. Indeed, fluorescence decay functions have been found for several specific forms of $\rho_{DA}(r)$, including a random 1-, 2-, 3-, and k-dimensional (fractal) distribution of acceptors around the donor molecule [4-6]. In biological applications treatments assuming a gaussian-type distributions [7,8] were also considered. The theory returns the analytical formula for the donor fluorescence decay function that is parametrically dependent on the assumed distribution. By fitting this formula to the experimental decay, the distribution parameters can be recovered. For example, assuming a random 3-D distribution of acceptors, namely $\rho_{DA}(r) \sim r^2$, results in the well known Förster formula $f_D(t) \sim \exp[-t/\tau_0 - 2\gamma(t/\tau_0)^{1/2}]$, where τ_0 is a fluorescence lifetime of a donor, and $\gamma = [A]/C_A$ is the ratio of the actual acceptor concentration $[A]$ to the critical acceptor concentration $C_A \sim R_0^{-3}$.

The approach described above, although useful and effective in numerous sensing applications [9,10] has two essential drawbacks. Firstly, the model fluorescence decay function, derived for the assumed $\rho_{DA}(r)$, is fitted to the experimental data in order to recover one unknown parameter ($[A]$) and also two other parameters, τ_0 and R_0, which, however, can be determined in separate experiments (τ_0 from the donor decay in the absence of acceptor and R_0 from the spectral overlap integral). In this sense, the experimental lifetime data are partially wasted. Moreover, the values τ_0 and R_0 recovered this way are correct only if the assumption regarding $\rho_{DA}(r)$ is correct, which is by definition a "hit or miss" affair! Indeed,

this approach frequently leads to inconsistency between R_0 determined from the spectral overlap integral (2) and from the time-resolved data analysed traditionally [11,12].
Secondly, in the complex biomedical/polymer FRET system, such as illustrated on Fig.2, it is very difficult to predict a realistic analytical expression for $\rho_{DA}(r)$. Moreover, even if we decide to choose one, the chance of deriving an analytical expression for the corresponding fluorescence decay function is very limited for mathematical reasons.

The alternative approach offered by FRET nanotomography [13-15] described here does not use an unsure form of $\rho_{DA}(r)$ to support fluorescence decay data to determine parameters (which can indeed be measured in separate experiments). Instead, it uses values of τ_0 and R_0 and the general properties of $\rho_{DA}(r)$ as the distribution function, as the only *a priori* information needed to support determination of $\rho_{DA}(r)$.

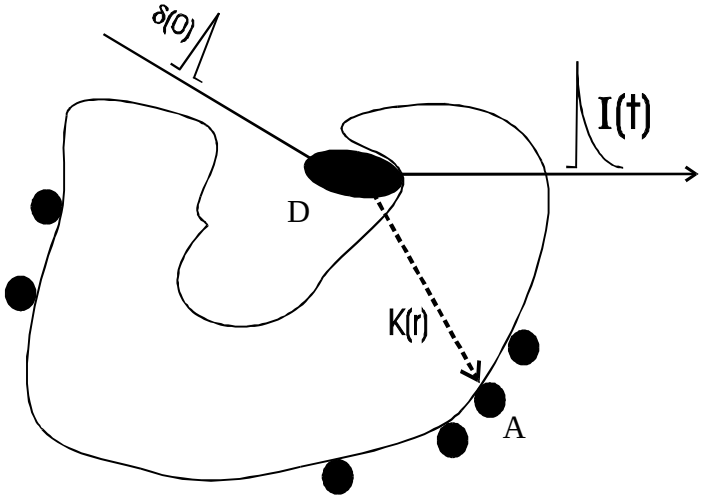

Fig.2. Schematic illustration of a typical biochemical structure with the donor (D) and acceptors (A) involved in FRET. Theoretical prediction of the $\rho_{DA}(r)$ and its evolution is very difficult.

2. FLUORESCENCE NANOTOMOGRAPHY

2.1. Fluorescence decay analysis for a general donor-acceptor distribution.

In the general case of the donor-acceptor distribution function $\rho_{DA}(r)$, the donor fluorescence decay function $f_D(t)$ within a so-called two-particle approximation [16] has a form

$$f_D(t) = \exp\left[-\frac{t}{\tau_0} - \int_0^\infty dr\,\rho_{DA}(r)\left(1-\exp\left[-tk(r)\right]\right)\right] \qquad (3)$$

By introducing [13]

$$f(t) = -\frac{t}{\tau_D} - \ln f_D(t) \qquad (4)$$

and $\alpha = R_0^6/\tau_0$, Eqtn. (3) can be rewritten in the form

$$f(t) = \int_0^\infty \left\{1-\exp\left[-\frac{\alpha t}{r^6}\right]\right\}\rho_{DA}(r)\,dr \qquad (5)$$

Here we demonstrate how introducing specific functional representation of the $\rho_{DA}(r)$, which reflect the general properties of $\rho_{DA}(r)$ as a distribution function, enables gaining structural information on the FRET system, namely determination of $\rho_{DA}(r)$ for $r<2R_0$. We assume the following general expression

$$\rho_{DA}(r) = \begin{cases} 0 & ,0 \le r \le a \\ R_0^{-1}\sum_{k=0}^{\infty} a_k^s L_k^s\left(\frac{r}{R_0}\right), & r > a \end{cases} \qquad (6)$$

where $L_k^s(r/R_0)$ are the orthonormal Laguerre polynomials represented by a series [17]

$$L_k^{(s)}(r) = \sum_{m=0}^{k} \frac{(-1)^m}{m!} \binom{k+s}{k-m} r^m \tag{7}$$

where $\binom{k}{m} = k(k-1)\ldots(k-m+1)/m!$ are the generalized binomial coefficients. An *a priori* feature added to the distribution function in the Eqtn. (6) is its zero value in the initial region $r \in (0,a)$, where $a < R_0$ is the minimum distance between the point dipoles representing the donor and acceptor molecules. Its value is verified during data analysis.

The Laguerre polynomials were chosen to represent the distribution function as they are defined in the region $(0,\infty)$ and because of their orthonormality, ensuring relatively simple and elegant integration. Also, the most common distribution functions, namely 1-, 2-, and 3-D random distributions, the last of them being an approximation of any donor-acceptor distance distribution at large distances, can be expressed by simple combinations of a few initial Laguerre polynomials.

Inserting the Eqtn(6) into Eqtn(5) and performing an integration over r gives

$$f(t) = \sum_{k=0}^{\infty} a_k^s \sum_{m=0}^{k} c_{km} \left(\frac{t}{\tau_0} \right)^{\frac{m+1}{6}} \tag{8}$$

where

$$c_{km} = \frac{(-1)^m}{(m+1)!} \binom{k+s}{k-m} \Gamma\left(\frac{5-m}{6}, \frac{a}{R_0} \right) \tag{9}$$

By introducing a new variable η

$$\eta(t) = \left(\frac{t}{\tau_0} \right)^{1/6} \tag{10}$$

the Eqtn. (8) converts to

$$F(\eta) = f(t) = \sum_{k=0}^{K} a_k^s \sum_{m=0}^{k} c_{km} \eta^{m+1} \tag{11}$$

where $K+1$ is the number of Laguerre polynomials used for the representation of the distribution function. By defining

$$b_m = \sum_{\substack{k=0 \\ k \geq m}}^{K} a_k^s c_{km} \tag{12}$$

we can rewrite the Eqtn. (11) as

$$F(\eta) = \sum_{m=0}^{K} b_m \eta^{m+1} \tag{13}$$

$F(\eta)$ is a polynomial of the $K+1$ power with $b_0=0$, thus $F(0)=0$. The b_m coefficients, if known, enable determination of the a_k^s parameters by solving the system of equations (12). On the other hand, $F(\eta)$ can be determined from the experimental data by making a parametric plot $(f(t), \eta(t))$, for t covering the experimental time window.

2.2. Numerical simulations.

In this section several model donor-acceptor distributions mimicking those occurring in real structural sensing applications are discussed and used in simulations. The purpose of these simulations is to test the spatial resolution of FRET nanotomography and to demonstrate its applicability for $\rho_{DA}(r)$ determination in molecular systems of dimensions comparable to R_0. It is important to highlight here, that although we use the theoretical expressions for $\rho_{DA}(r)$ in simulations, FRET nanotomography applied to the real data does not require making any assumptions regarding the form of $\rho_{DA}(r)$ at any stage of data analysis.

We will shortly review the 1-,2-,3- and k-dimensional random distributions of acceptors around a single donor molecule (leading to the classical Förster-type analytical solutions for $f_D(t)$), and the class of spherically symmetric distributions, which can be regarded as the first approximations of the distributions occurring in porous materials and numerous macromolecular systems.

The simulations were performed as follows. For a given $\rho_{DA}(r)$ and chosen τ_0 and R_0 values, the resulting $f_D(t)$ was calculated numerically according to the Eqtn (3). In order to simulate the results of the reconvolution of the real data, the model $f_D(t)$ was then fitted to multiexponential (usually 5-exponential) function and included into the procedure described in Section 2.1.

2.2.1. Appropriate choice of R_0 for the spatial scale of $\rho_{DA}(r)$.

We assume here a normal donor-acceptor distribution function $\rho(r)$

$$\rho(r) = \frac{\alpha}{\sqrt{\pi}}\left(\frac{r}{d}\right)^2 \exp\left[-\alpha^2 (d-r)^2\right] \qquad (14)$$

(solid line in Fig.3), where α=0.5 nm^{-1} and d=5 nm. For a fixed τ_D=2.5 ns and the different R_0 values equal to 1, 1.5, 2, 4 and 6 nm the distribution was then recovered (dotted lines). The result confirms clearly the intuitive prediction, that the critical transfer distance R_0 establishes the spatial range of the sensor. Indeed, the method seems to reproduce properly $\rho_{DA}(r)$ in the region $a<r<2R_0$, though obviously not in the region $0<r<a$ where the Förster transfer efficiency is close to unity (see Eqtn(1)). The small deviations of the dotted line from a solid one (real distribution) obtained for R_0=6 nm are the result of using a limited number of components in the series given by Eqtn (6) (usually 12-14), and approximate representation of the calculated decay by a 5-exponential function. However, even for large number of components of Eqtn (6) and high number of exponentials, an accurate determination of $\rho_{DA}(r)$ for $r<<R_0$ or $r>>R_0$, cannot be expected. In further analysis we investigated the region $r<2R_0$ only.

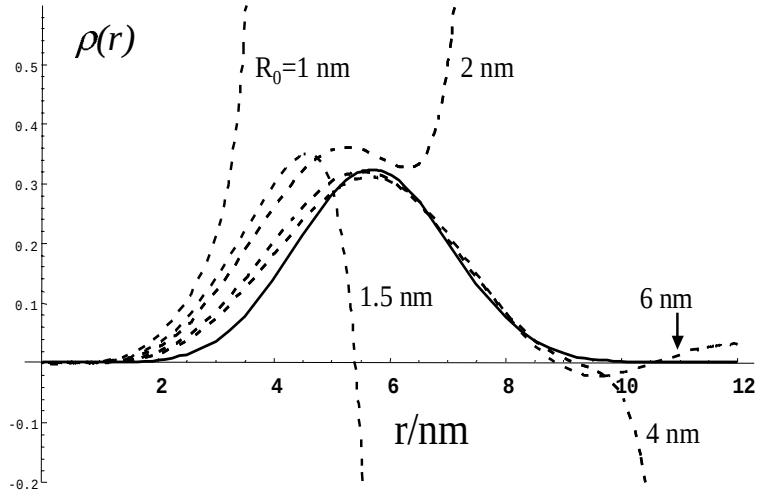

Fig.3. Assumed normal donor-acceptor distribution function (solid line) and the recovered distribution functions (dashed lines) for R_0=1,1.5,2,4 and 6 nm.

2.2.2. Random distributions.

The simplest donor-acceptor distribution occurs for a very low donor concentration, *[D]<<[A]*, and for the acceptors randomly distributed in *k*-dimensional space

$$\rho_{DA}(r) = kV_k \rho r^{k-1} \qquad (15)$$

where V_k is the volume of the unit sphere in *k* dimensions and ρ has a meaning of the number of acceptors per volume unit. Insertion (15) into (3) gives

$$f_D(t) = \exp[-t/\tau_0]\exp\left[-V_k \rho R_0^k \Gamma(1-k/6)(t/\tau_0)^{k/6}\right] \qquad (16)$$

This general solution contains several particular cases considered in earlier papers [11,12], including the Förster expressions for 1-, 2-, and 3-dimensional geometries. All the models discussed above are only strictly applicable under well defined kinetic conditions and in the case of complex heterogeneous environments such as permeable polymer matrices or in biological material such as whole cells or sub-cellular structures they can only be considered as approximate. For the purpose of this work, we will use the formula (16) to investigate whether FRET nanotomography

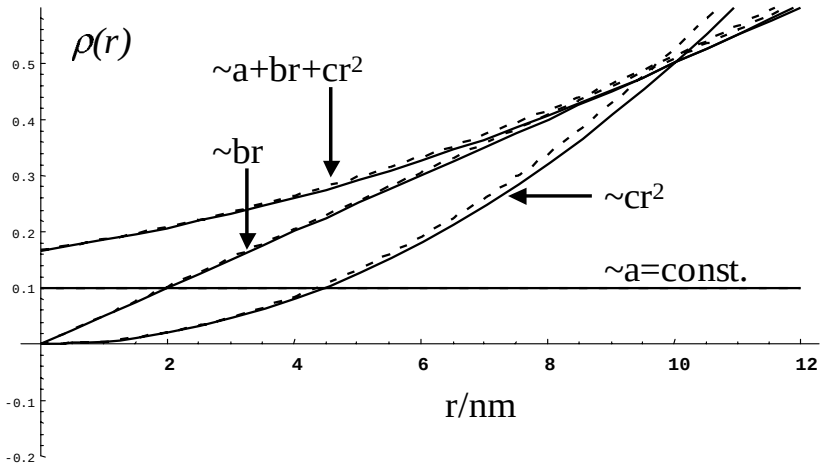

indeed returns the distribution (15) as the response. Figure 4 presents the assumed and recovered distribution functions corresponding to the random 1-D, 2-D, 3-D, and mixed distributions of acceptors. The very good consistency occurring here is a consequence of the assumed functions being easily represented by a few initial Laguerre polynomials only, eg for the mixed distribution $a_0,a_1,a_2 \neq 0$ and for $i>2$ $a_i=0$. Because any $\rho_{DA}(r)$ becomes $\sim r^2$ at large distances, this feature of a_i coefficients is one of key advantages of using Laguerre polynomials to represent distribution functions.

Fig.4. The assumed (solid lines) and recovered (dashed lines) distribution functions for the random 1D, 2D, 3D and mixed donor-acceptor distance distributions.

2.2.3. δ-type donor and normal-acceptor distribution.

Conformational changes of macromolecules like proteins and DNA chains, are a well established application of FRET. In these systems FRET kinetics usually involve complex distributions of intrinsic or specially attached donors and acceptors. For our purposes we consider a model macromolecule characterised by a δ-type distribution of donors and normal distribution of acceptors

$$\rho_D(r) = \delta(r-\Delta) \tag{16}$$

$$\rho_A(r) = \frac{4\alpha^3 r^2}{\sqrt{\pi}} \exp\left[-\alpha^2 r^2\right] \tag{17}$$

Here Δ is an average donor-acceptor separation and α=0.25 nm^{-1} is a measure of the acceptor spread. The mutual donor-acceptor distribution is then [18]

$$\rho_{DA}(r) = \frac{\alpha r}{\sqrt{\pi}\Delta} \exp\left[-\alpha^2 (\Delta - r)^2\right] \tag{18}$$

The recovered functions properly reproduce the assumed $\rho_{DA}(r)$ in the region from 0 to about 10 nm, confirming again the suitability of the method for the analysis of macromolecular structures.

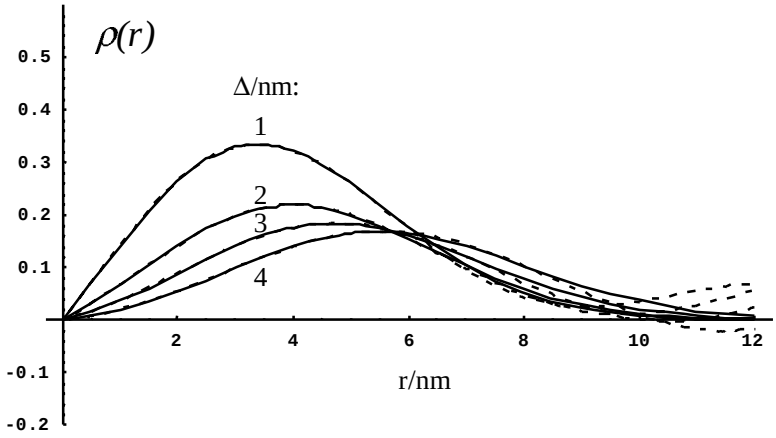

Fig.5. The δ-type donor and normal-acceptor distribution function for different average donor-acceptor separations Δ=1,2,3 and 4 nm.

2.2.4. Effect of the minimum donor-acceptor distance.

In the Förster theory the model distribution functions (15) are >0 for *r* varying from 0 to infinity, including very small r values, resulting in a non-realistic case of overlapping donor and acceptor molecules. This effect is negligible for donor and acceptor dimensions much smaller than R_0 but clearly cannot be neglected for those donor/acceptor/medium systems, where the minimum possible donor-acceptor separation is comparable with R_0. In this case, not including molecular sizes into a model distribution function can lead to overestimating the rate of FRET. Actually, experimental evidence on numerous FRET systems we investigated [19] showed that R_0 determined from lifetime measurements according to Eqtn(16), is lower than R_0 calculated from the spectral overlap integral, Eqtn(2).

A simple model of a distribution function that includes a minimum donor-acceptor separation R_{min}, $\rho_{DA}(r) \sim (r-R_{min})^2$, is presented in Fig.6. The recovered curves (dotted lines) are in good agreement with the assumed distributions, demonstrating potential of FN to detect the minimum donor-acceptor separation. This is particularly useful in material structure determination, as we demonstrate in section 3.2 for a porous polymer Nafion 117.

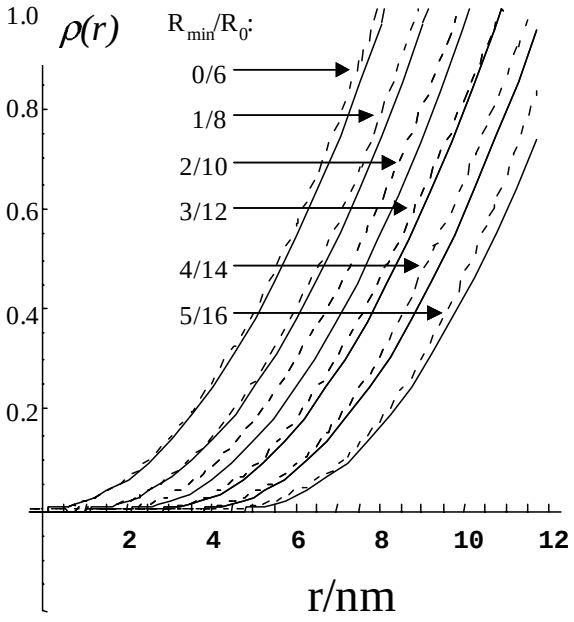

Fig.6. Effect of the minimum donor-acceptor distance R_{min}.

2.3. Experimental requirements for FN.

Fluorescence decay functions were measured using a standard single photon timing technique of sub-nanosecond time resolution (Fig.7). Investigated systems contained intrinsic or specially bound donor and acceptor molecules. Numerical simulations of this technique allowed establishing additional experimental conditions specific for FN. They include:

1. Donor fluorescence decay should be mono-exponential in the absence of the acceptor.
2. The critical transfer distance R_0 should be of the same range as the characteristic dimensions of the investigated structure.
3. The closer donor-acceptor distance in the system, the shorter the donor lifetime required (and consequently better time resolution).

Data analysis was performed using in the first stage the IBH iterative reconvolution software with the chi-squared (χ^2) test used to assess the goodness of fit. The donor decay after reconvolution represented by a 5-exponential function was then used in the procedure described in section 2.1. In each experiment τ_0 was measured separately from the donor decay in the absence of acceptor and R_0 from the spectral overlap integral.

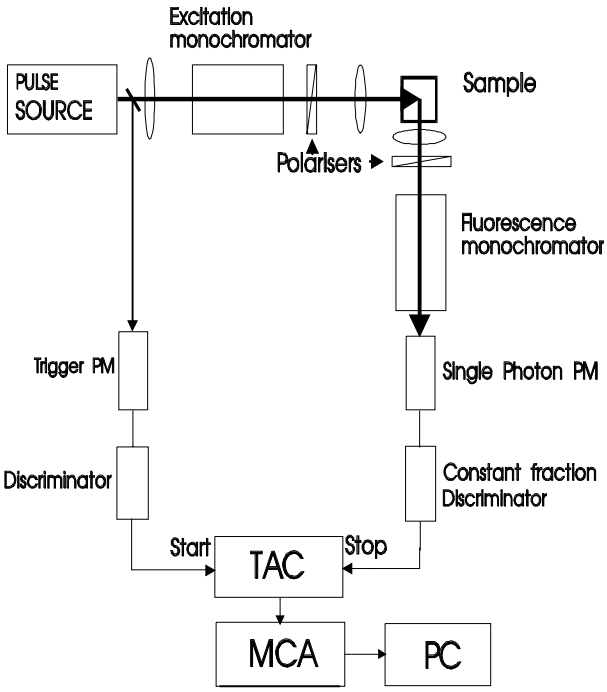

Fig.7. A typical fluorescence lifetime set-up is adequate for FN. A Hamamatsu PLP-01 diode laser operated at 10 MHz repetition rate was used for excitation. Emission was collected using a cut-off filter. Prism polarisers were used at magic angle. The maximum number of counts in a channel was 10,000 recorded at a channel width of 48.2 ps/ch.

3. FN APPLICATION.

In this section we demonstrate applications of FN to the different FRET systems which are currently under investigation in our lab. Each plot of the experimental $\rho_{DA}(r)$ is followed by a molecular model consistent with this result.

3.1. 3-D random donor-acceptor (D-A) distribution.

The FN method was tested by using a donor-acceptor pair in a solution, for which a random 3D distribution was previously confirmed by giving a perfect fit to Förster analysis [20]. A near-infrared dye DTDCI was used as a donor and the hydrated copper ion $Cu{\cdot}5(H_2O)^{2+}$ as an acceptor. A viscous solvent propylene glycol was used to avoid any diffusional effects. Figure 8 demonstrates a parabolic shape of the recovered distribution function (see inset shoving linear $\rho_{DA}(r)$ vs r^2 dependence), indicating a random distribution of copper ions around a DTDCI molecule.

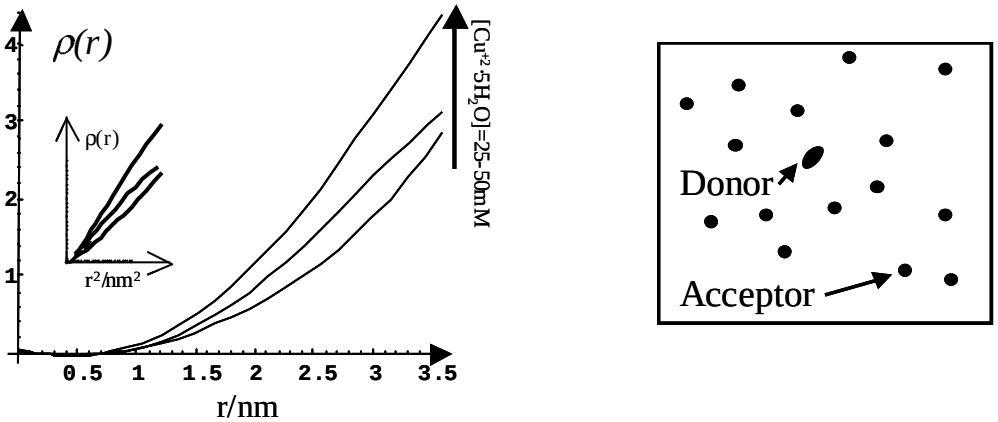

Fig.8. A random distribution of the hydrated copper ions around a near-infrared molecule DTDCI in propylene glycol. The critical transfer distance for the DTDCI-Cu^{2+} pair is 19.5 Å.

3.2. D-A distribution in a polymer matrix.

The same DTDCI-Cu pair was used in a polymer matrix Nafion 117 ®, where we expected to see some deviations from a random distribution, which would reflect a polymer morphology [21]. In water-doped Nafion the critical transfer distance R_0 is 19.2 Å, which corresponds well to the estimated averaged radius of the Nafion water pools of 20 Å. Data revealed (Fig.9.) a 5 Å barrier to the metal ions accesing the donor in Nafion 117 probably caused by donor molecules being trapped in the narrow channels of the polymer and the metal ions distributed randomly in the water pools.

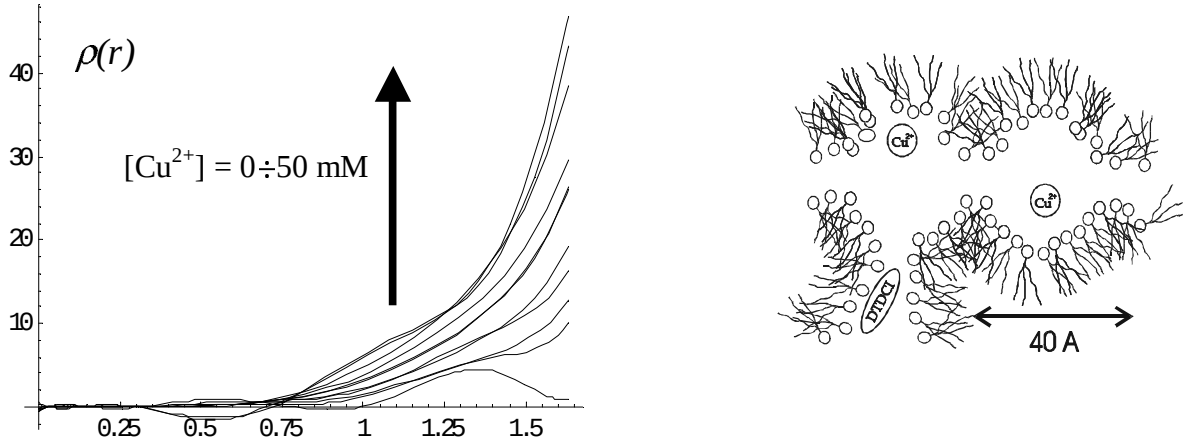

Fig.9. DTDCI-Cu^{2+} distribution in a polymer Nafion 117.

3.3. D-A complexes.

When dimensions of the interacting molecules are comparable to the R_0, a random D-A distribution cannot be expected. We used a fluorescent protein Allophycocyanin (APC) of the diameter 110 Å as a donor and a small non-fluorescent dye malachite green (MG) as an acceptor [22]. The R_0 for this pair is 59.8 Å, which is only a half of the donor dimension. Consequently, the resulting distribution (Fig.10) is far from random distribution. The result is consistent with donor randomly distributed within a sphere and acceptor on the surface of the sphere.

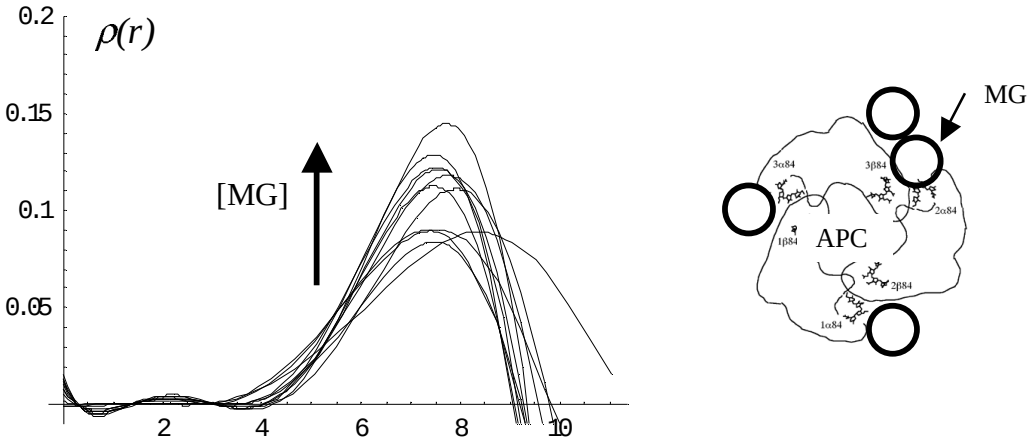

Fig.10. APC-MG distribution function in a bulk solution (PBS buffer).

3.4. Protein interactions.

FN also confirmed its usefulness in molecular glucose sensing. We used a sensor based on a well researched principle of competitive binding of dextran and glucose to the sugar binding sites in ConcanavalinA (ConA). ConA in our sensor was labelled by APC (donor) and dextran by MG (acceptor) [9,14,23,24]. In the absence of glucose binding sites are occupied by acceptor-labelled dextran molecules. This results in a small donor-acceptor distance and thus efficient FRET. On the appearance of glucose, some labelled dextran molecules are removed from the binding sites and a new donor acceptor distance distribution is established by the dynamic equilibrium between glucose and dextran molecules.

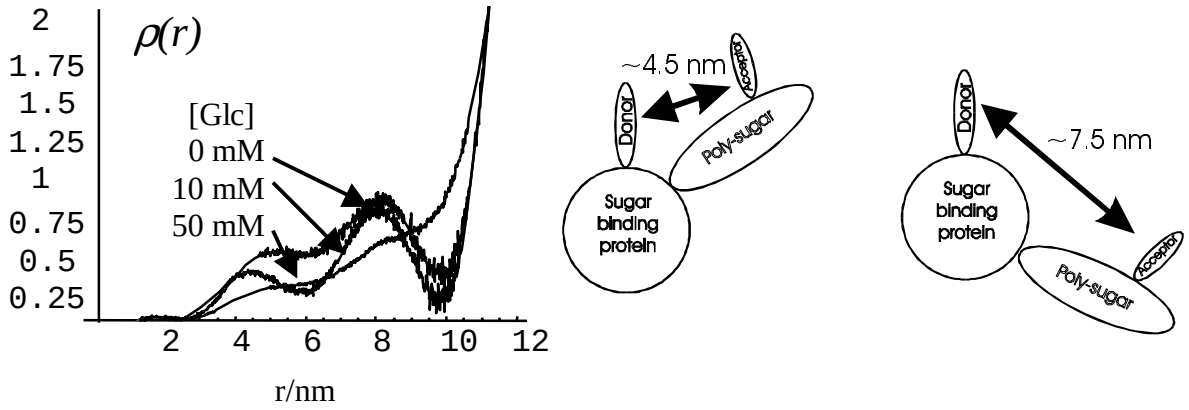

Fig.11. APC-MG distribution functions for 0,10 and 50 mM glcose.

Figure 11 demonstrates the $\rho_{APC\text{-}MG}(r;[Glc])$ functions for three values of glucose concentration recovered from the fluorescence decays. The result shown indicates that the minimum donor-acceptor distance is about 25 Å. The main features of the distribution functions revealed in this approach, are two maxima at ~4.5 nm and at ~7.5 nm and a parabolic dependence at larger distances. The existence of two maxima in the APC-MG distribution function indicate two types of APC-ConA:Dextran-MG complexes resulting in two characteristic APC-MG distances. This is consistent with the presence of four sugar binding sites in a ConA tetramer.

3.5. Lipid bilayer membranes.

We used FN to study perylene in DPPC phospholipids in an attempt to solve a long standing problem as to where aromatic dyes go in liposomes. Small unilammellar vesicles were prepared using ethanol injection. Lipid and perylene stock solution were dissolved in ethanol at the required lipid to dye ratio (200:1) and then injected in to phosphate buffer at 328K, which was above the phase transition temperature for DPPC. The hydrated cobalt ions $Co{\cdot}6(H_2O)^{2+}$ were used as acceptor, giving R_0=10.7 Å.

Our preliminary data (Fig.12) show two peaks in the distribution function at 1.25 and 2.25 nm,which is tentatively interpreted as corresponding to acceptors on the inner and outer vesicle walls, respectively. The resulting total bilayer width 1.25nm + 2.25nm = 3.5nm is consistent with electron microscopy measurements on the dry colloid. The dye is found to be located more towards the inner wall. Once fully developed FN would seem to offer a promising new approach to studying membrane structure, dynamics and interactions.

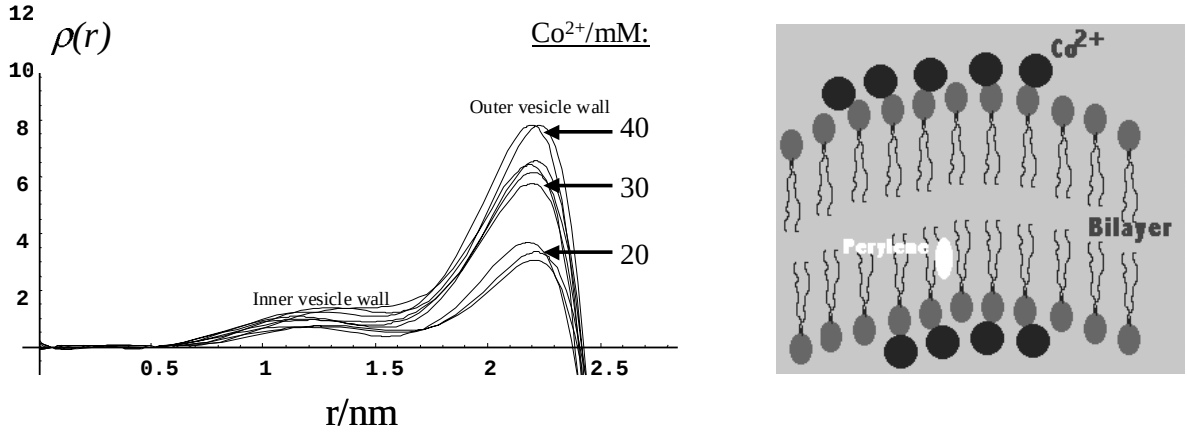

Fig.12. Perylene-cobalt distribution function in DPPC phospholipids.

ACKNOWLEDGEMENTS

The authors wish to thank The Wellcome Trust and EPSRC for financial support and C Mathivanan for his help in phospholipid lifetime measurements.

REFERENCES

1. T.Förster, "Experimentelle und theoretische Untersuchung des zwischenmolekularen Ubergangs von Elektronenanregungsenergie", Z.Naturforsch. 4a (1949) 321-327.
2. L.Tolosa, H.Szmacinski, G.Rao and J.R.Lakowicz, "Lifetime-based sensing of glucose using energy transfer with a long-lifetime donor", Anal.Biochem. 250 (1997) 102-108.
3. R.M.Bevensee, *Maximum entropy solutions to scientific problems*, PTR Prentice Hall, Englewood Cliffs, 1993.
4. J.Klafter, J.M.Drake and A.Blumen, in M.Grätzel and K.Kalyanasundaram (Edts.), *Kinetics and catalysis in microheterogeneous systems*, Marcel Dekker, Inc., New York, 1991, Chapter 14.
5. N.L.Vekshin, *Energy transfer in macromolecules*, SPIE Press, Bellingham, 1997.
6. A.Blumen, J.Klafter and G.Zumofen, "Influence of restricted geometries on the direct energy transfer", J.Chem.Phys., 84, 3 (1986) 1397-1401.
7. J.R.Lakowicz, *Principles of fluorescence spectroscopy*, Ch.14, pp. 395-423, Kulwer Academic, New York, 1999.
8. P.Wu and L.Brand, " Resonance energy transfer: Methods and applications ", Biochemistry, 33 (1994) 10457.
9. L.J.McCartney, J.C.Pickup, O.J.Rolinski and D.J.S. Birch, "Near-infrared fluorescence lifetime assay for serum glucose based on allophycocyanin-labelled concanavalin A, Anal.Biochem., 292 (2001) 216-221.
10. O.J.Rolinski, D.A.Hatrick, A.Volkmer and D.J.S. Birch, "The photophysics of xanthene dyes in Nafion polymer membrane: Application to copper sensing", Jour. of Fluorescence, 7 (1997) 207-209.
11. O.J.Rolinski and D.J.S.Birch, "A fluorescence lifetime sensor for Cu(I) ions", Meas.Sci.Technol., 10 (1999) 127-136.
12. O.J.Rolinski, D.J.S.Birch and A.S.Holmes, "Metal ion quenching kinetics of DTDCI in viscous solution and Nafion membranes: A model system for near infra-red fluorescence sensing", J.Biomed.Optics, 3 (1998) 346-356.
13. O.J.Rolinski and D.J.S.Birch, "Structural sensing using fluorescence nanotomography", J.Chem.Phys. 116, 23 (2002) 10411-10418.
14. O.J.Rolinski, D.J.S.Birch. L.McCartney and J.C.Pickup, "Fluorescence nanotomography using resonance energy transfer: Demonstration with a protein-sugar complex", Phys.Med.Biol. 46 (2001) N221-N226.

15. O.J.Rolinski and D.J.S.Birch, "Determination of acceptor distribution from fluorescence resonance energy transfer. Theory and simulation", J.Chem.Phys., 112, 20 (2000) 8923-8933.
16. S.Murata and M.Tachiya, "Transient effect in fluorescence quenching by electron transfer .3. Distribution of electron transfer distance in liquid and solid solutions", J.Phys.Chem., 100 (1996) 4064-4070.
17. I.S.Gradshteyn and I.M.Ryzhik, *"Tables of Integrals, Series, and Products"*, A.Jeffrey (Ed.), Academic Press, San Diego, 1994.
18. A.V.Barzykin, "Spatial distribution of probes in a micelle: effects on the energy transfer time-resolved measurables", Chem.Phys., 155 (1991) 221-231.
19. D.J.S.Birch and O.J.Rolinski, "Fluorescence resonance energy transfer sensors", Res.Chem.Intermed., 27, 4-5 (2001) 425-446.
20. O.J.Rolinski, I.R.Downie, A.S.Holmes and D.J.S.Birch, "The potential use of IR dyes for metal ion sensors", SPIE Proc., 2388 (1995) 290-301.
21. W. J. O'Hagan, M. McKenna, D. C. Sherrington O. J. Rolinski and D. J. S. Birch**, "**MHz LED source for nanosecond fluorescence sensing", Meas.Sci.Technol., 13 (2002) 84-91.
22. O.J.Rolinski, D.J.S.Birch, L.J.McCartney and J.C.Pickup, "Fluorescence resonance energy transfer from allophycocyanin to malachite green", Chem.Phys.Lett., 309 (1999) 395-401.
23. O.J.Rolinski, D.J.S.Birch, L.J.McCartney and J.C.Pickup, "Molecular distribution sensing in a fluorescence resonance energy transfer based affinity assay for glucose", Spectrochim.Acta., A 57 (2001) 2245-2254.
24. O.J.Rolinski, D.J.S.Birch, L.J.McCartney and J.C.Pickup, "A time-resolved near infra-red florescence assay for glucose: opportunities for trans dermal sensing" J.Photochem.Photobiol.B, 54 (2000) 26-34.